Supplementary information for

Highly dispersed and functionalized boron nitride nanosheets contribute to ultra-stable long-life all-solid-state batteries

Jiawei Ji, Hongliang Duan, Zheng Zhou, Chaoze Liu, Dong Wang, Song Yan, Shaobo Yang, Wenjuan Bai, Yanming Xue*, Chengchun Tang*

School of Materials Science and Engineering, Hebei University of Technology, Tianjin 300130, PR China

Hebei Key Laboratory of Boron Nitride and Nano Materials, Hebei University of Technology, Tianjin 300130, PR China

*Corresponding E-mail addresses: ym.xue@hebut.edu.cn and tangcc@hebut.edu.cn

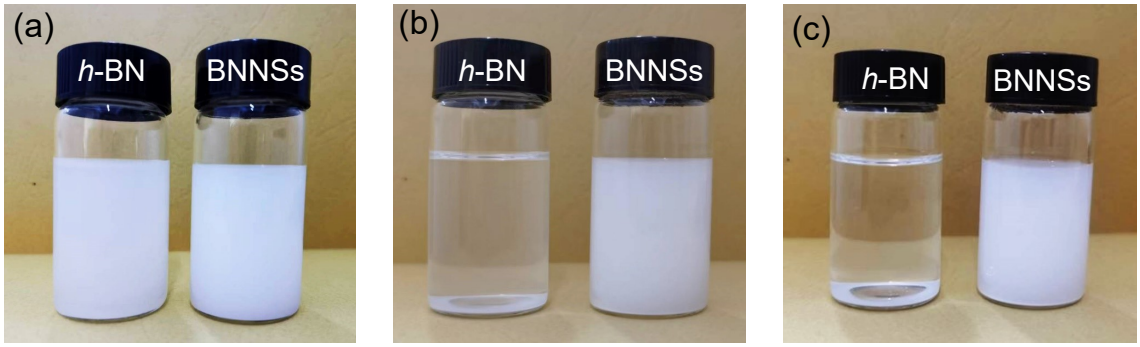

Figure S1 The photo of h-BN and BNNSs (1 mg/ml) in AC (a), after 1 h (b); after 24 h (c)

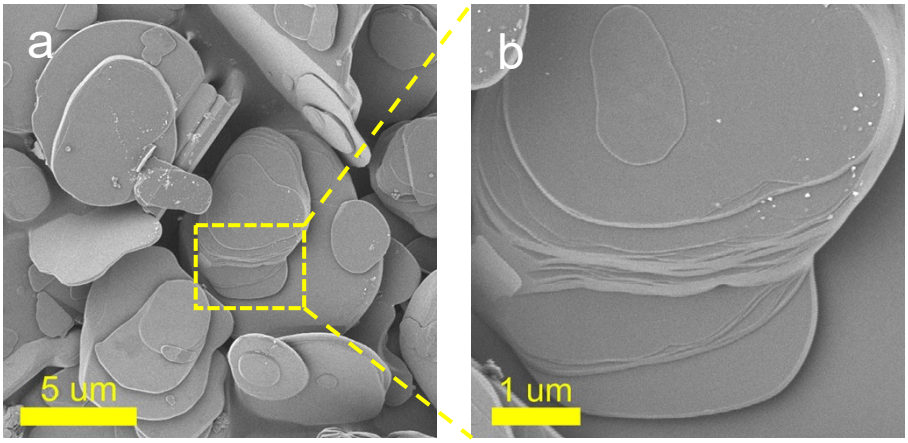

Figure S2 SEM images of *h*-BN

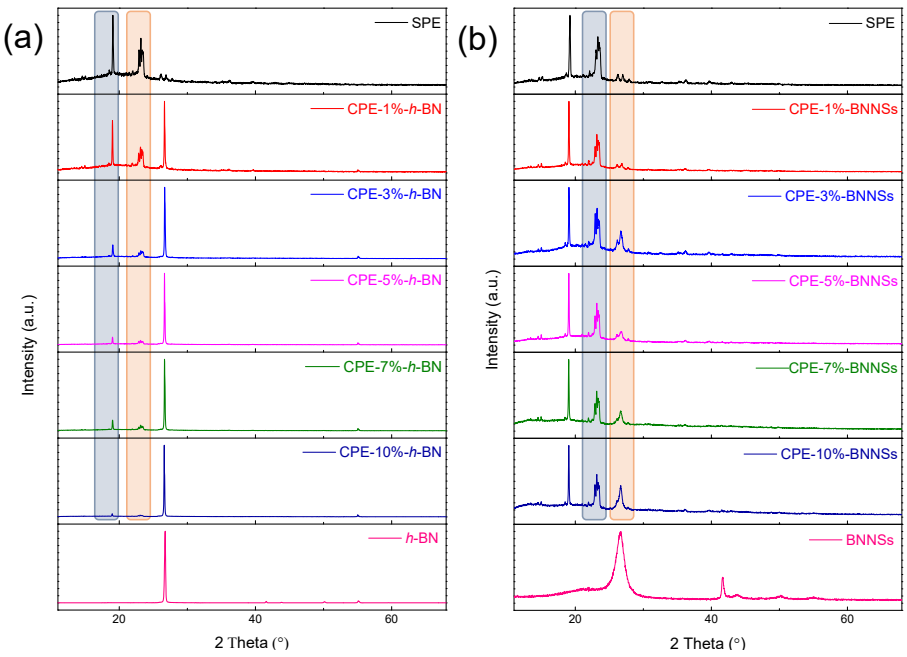

Figure S3 XRD patterns of CPE-*h*-BN (a) and CPE-BNNSs (b) at different contents

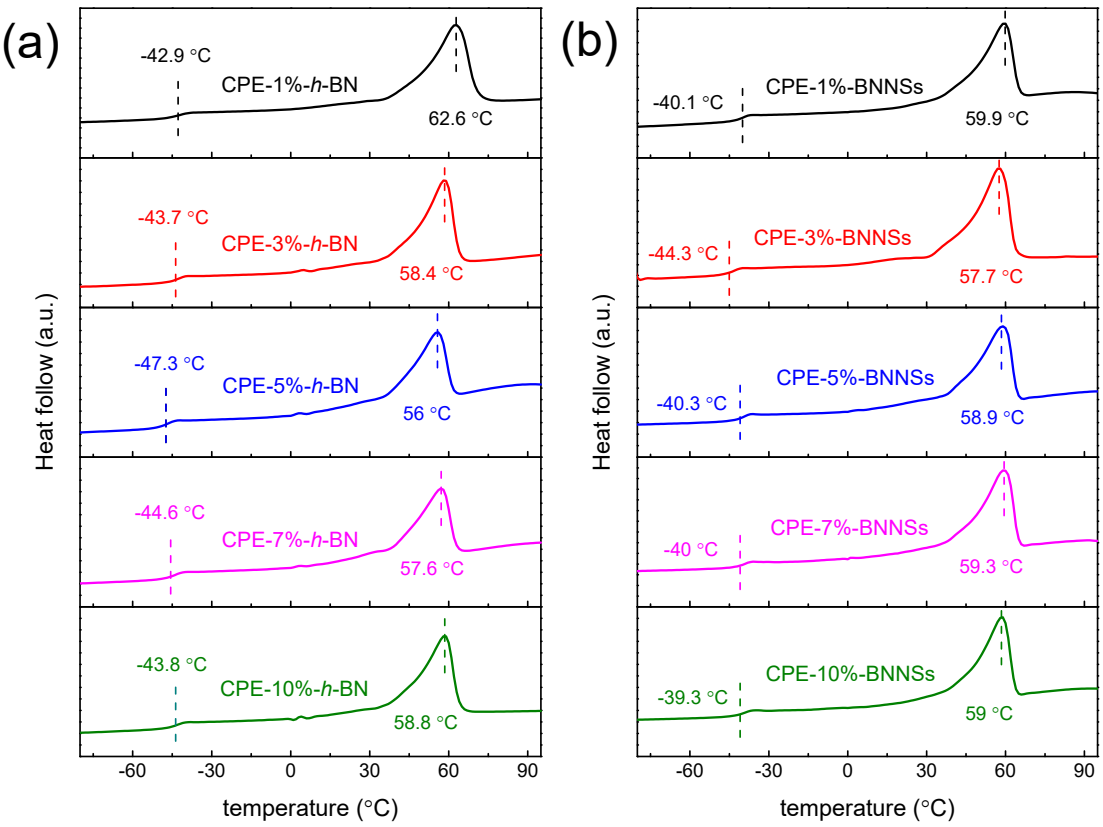

Figure S4 DSC thermograms of CPE-h-BN (a) and CPE-BNNSs (b) at different contents in the temperature from -80 °C to 95 °C

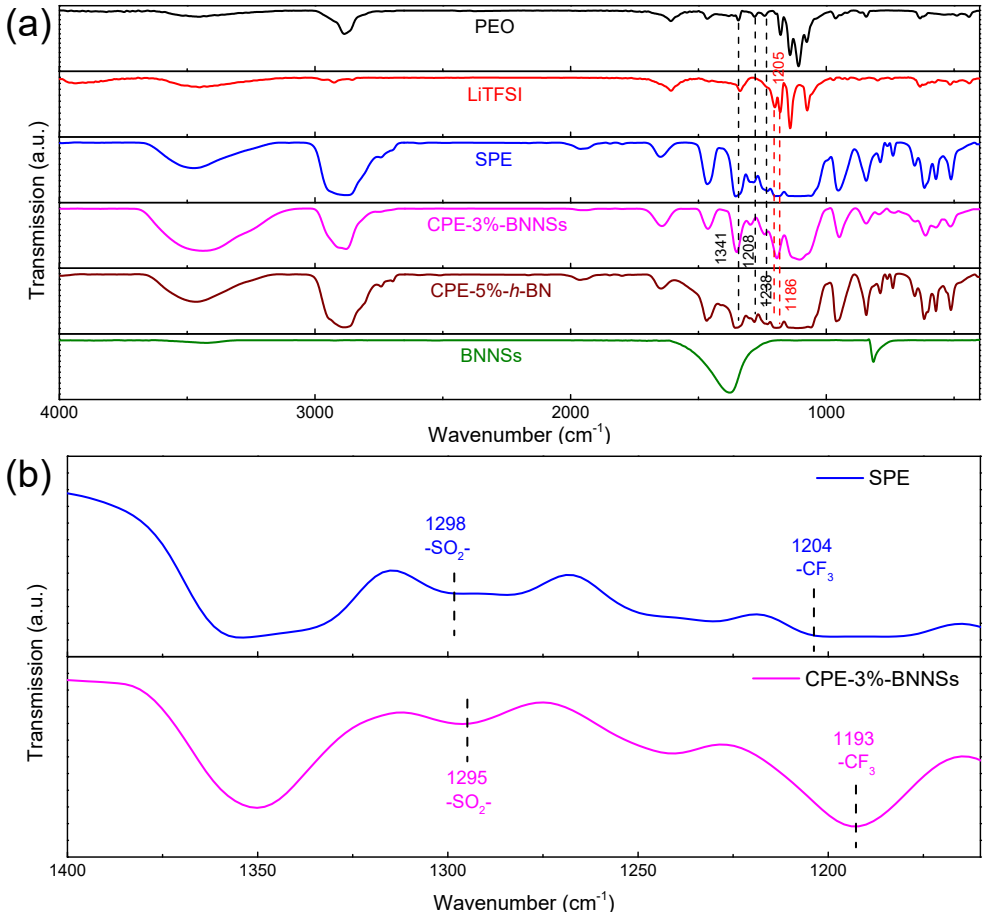

Figure S5 FTIR spectra of PEO, LiTFSI, SPE, CPE-3%-BNNSs, CPE-5%-*h*-BN and BNNSs (a); detail FTIR spectra of SPE and CPE-3%-BNNSs range from cm^{-1} 1400 to 1160 cm^{-1}

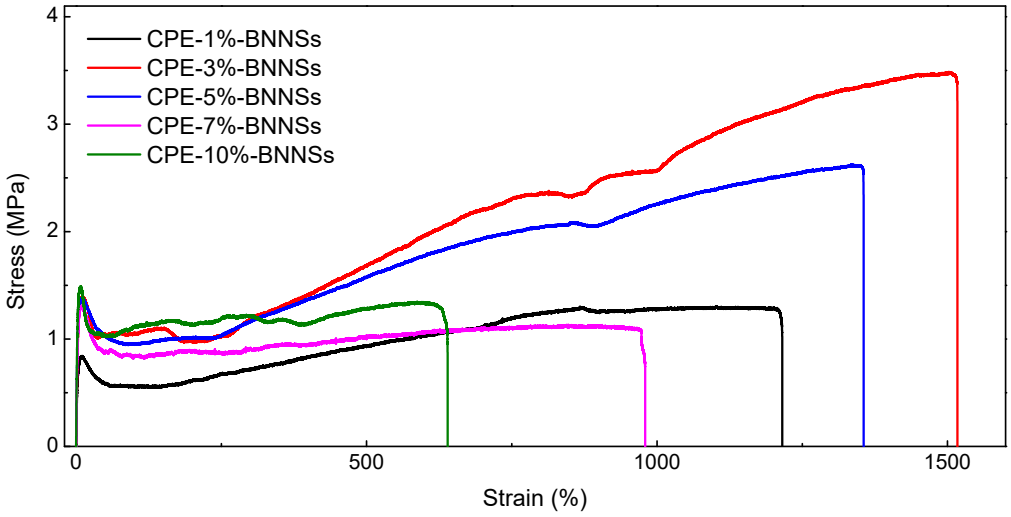

Figure S6 Stress-strain curves of CPE-BNNSs membrane at different contents

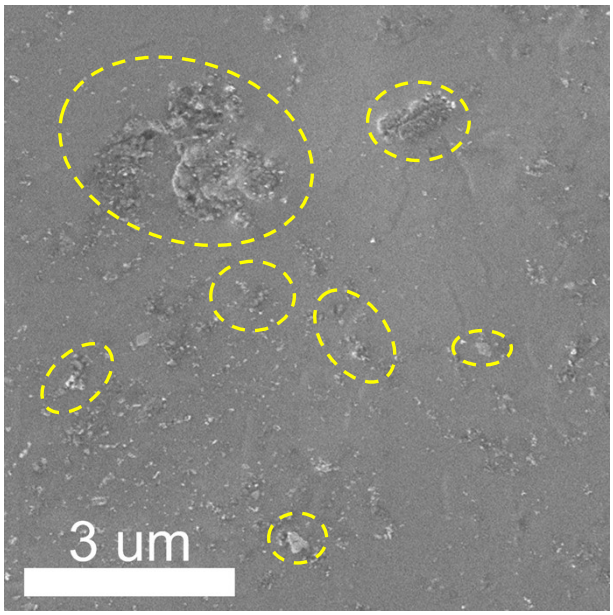

Figure S7 SEM image of CPE-5%-*h*-BN

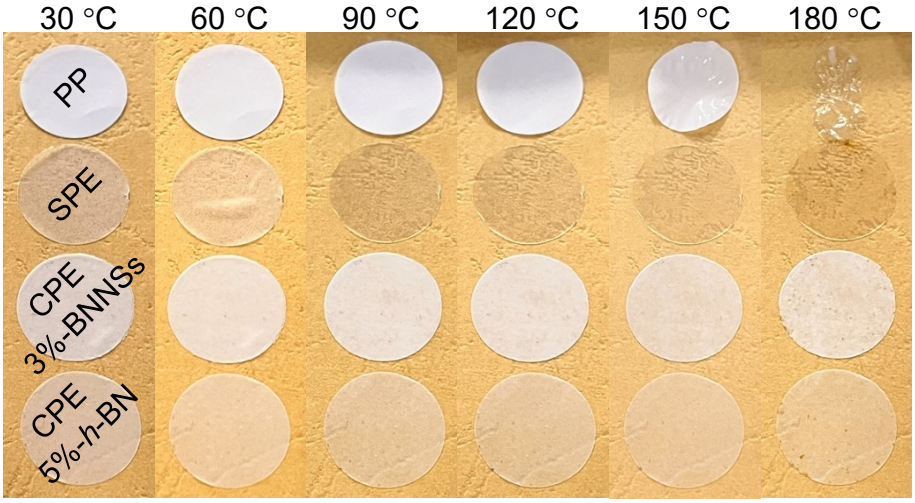

Figure S8 The optical photos of Celgard 2325 membranes, SPE, CPE-3%-BNNSs and CPE-5%-h-BN at different temperatures

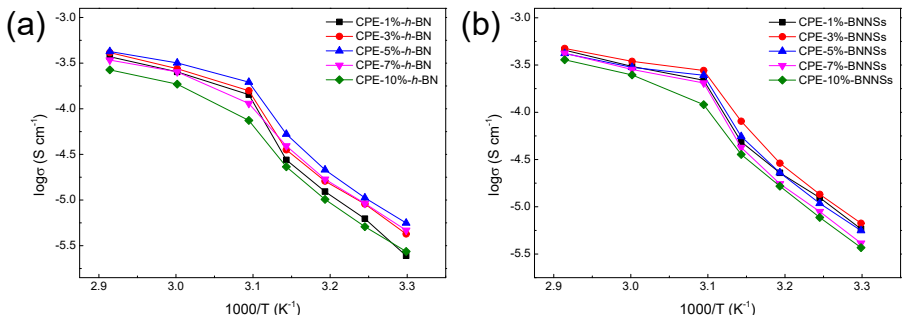

Figure S9 Ionic conductivities of CPE-h-BN (a) and CPE-BNNSs (b) at different contents in the temperature from 30°C to 70 °C

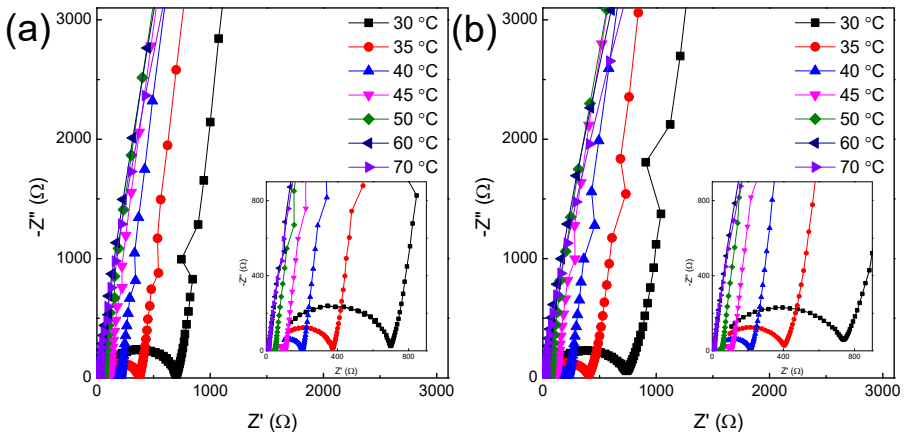

Figure S10 EIS spectrum of CPE-5%-h-BN (a) and CPE-3%-BNNSs with a symmetrical blocking cell at different temperatures

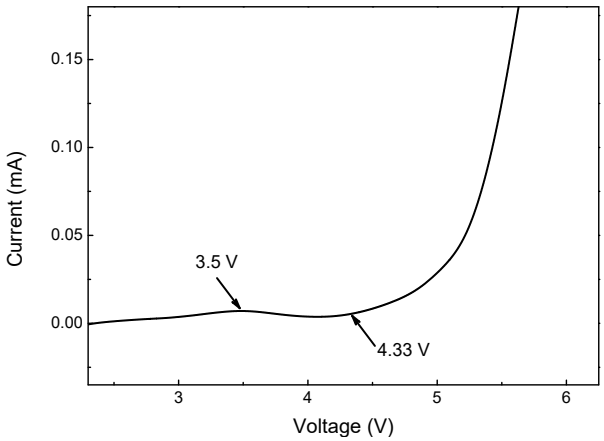

Figure S11 LSV curves of CPE-3%-*h*-BN films at 60 °C

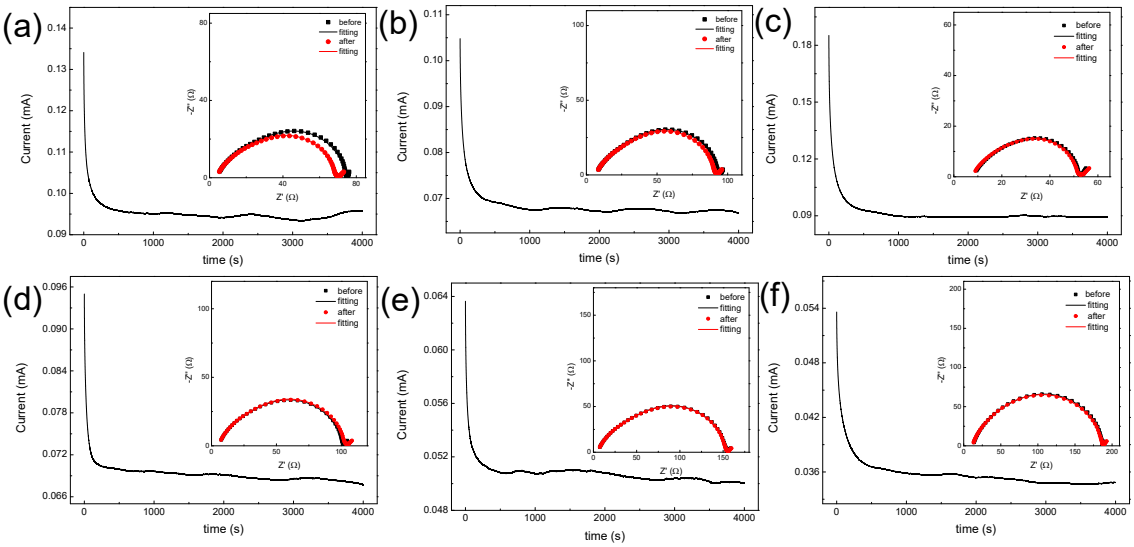

Figure S12 Chronoamperometry curves of SPE (a), CPE-1%-*h*-BN (b), CPE-3%-*h*-BN (c), CPE-5%-*h*-BN (d), CPE-7%-*h*-BN (e) and CPE-10%-*h*-BN films at a potential step of 10 mV and a duration time of 4000 s at 60 °C, the inset figure shows EIS of same cell before and after polarization

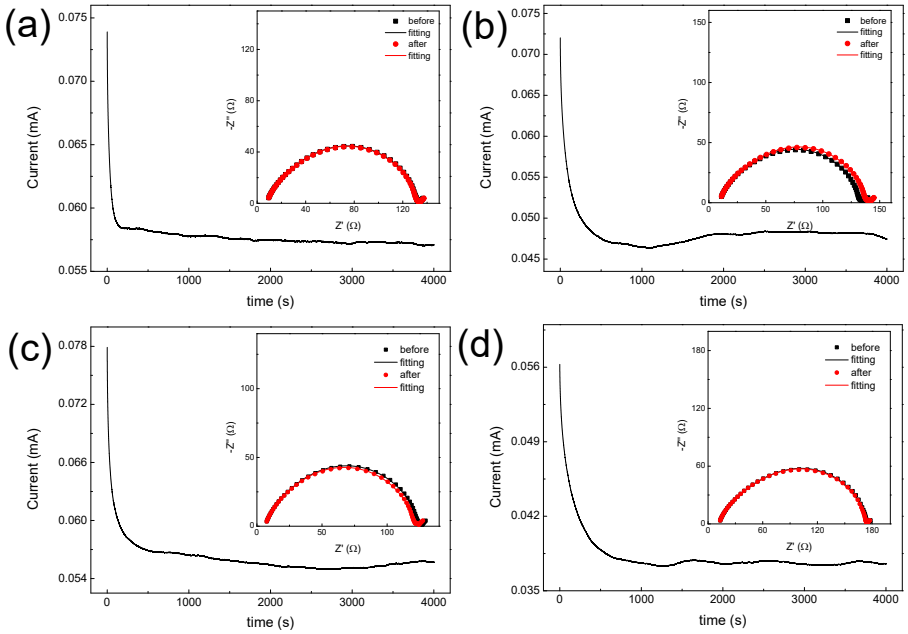

Figure S13 Chronoamperometry curves of CPE-1%-BNNSs (a), CPE-5%-BNNSs (b), CPE-7%-BNNSs (c) and CPE-10%-BNNSs films at a potential step of 10 mV and a duration time of 4000 s at 60 °C, the inset figure shows EIS of same cell before and after polarization

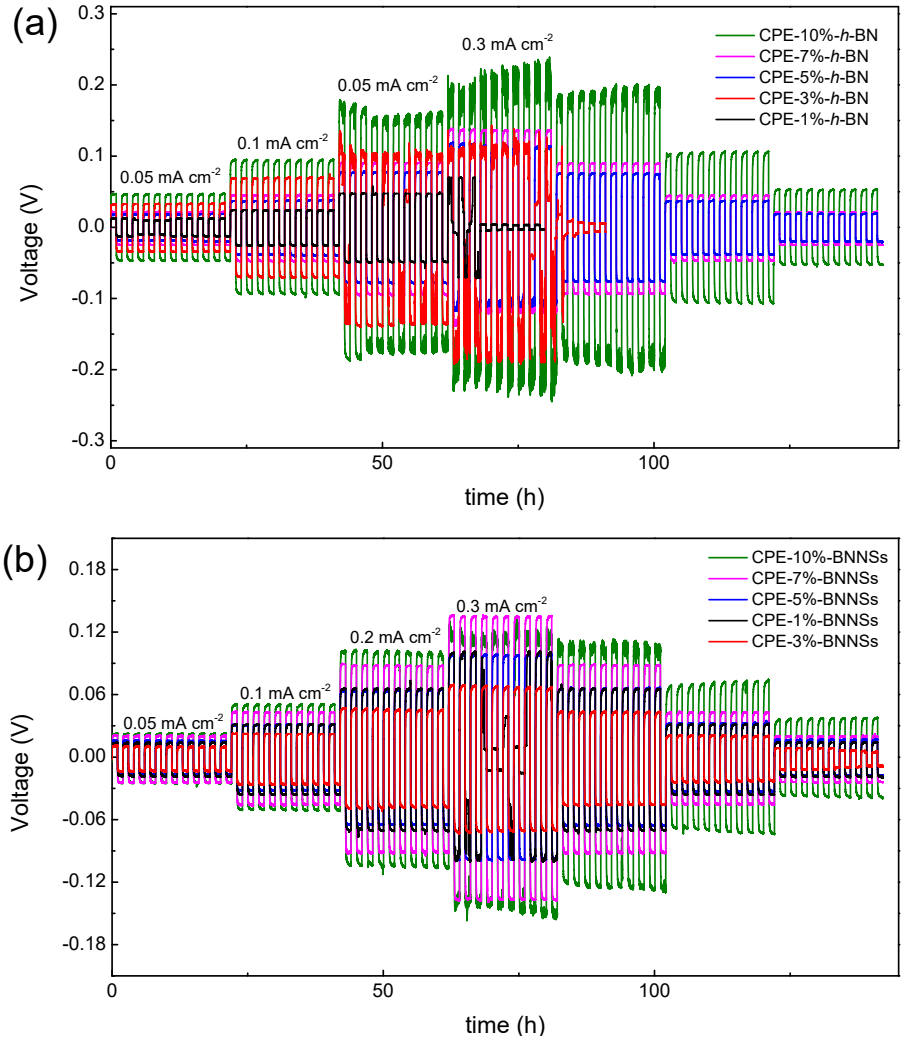

Figure S14 Lithium plating and striping experiment of symmetric cells with CPE-h-BN and CPE-BNNSs at current densities of 0.05, 0.1, 0.2 and 0.3 mA cm^{-2} (0.101 mA, 0.201 mA, 0.402 mA，0.603 mA,) at 60 °C

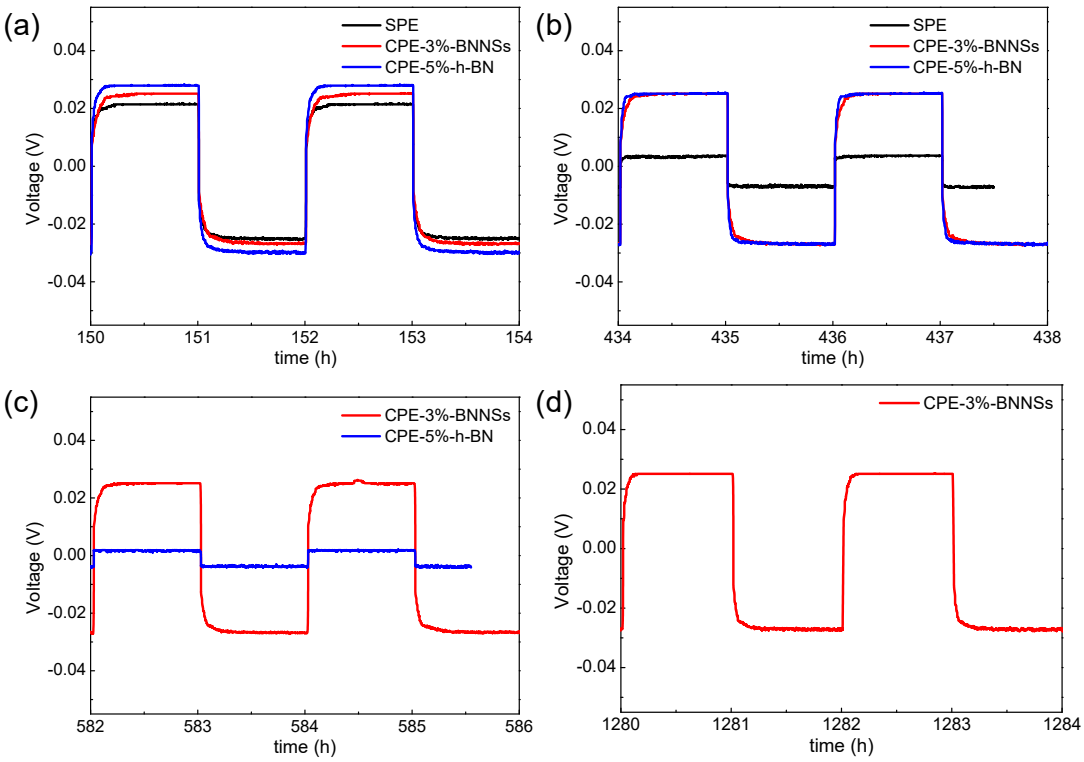

Figure S15 The enlarge diagram of the voltage profiles at different time of SPE, CPE-5%-*h*-BN and CPE-3%-BNNSs

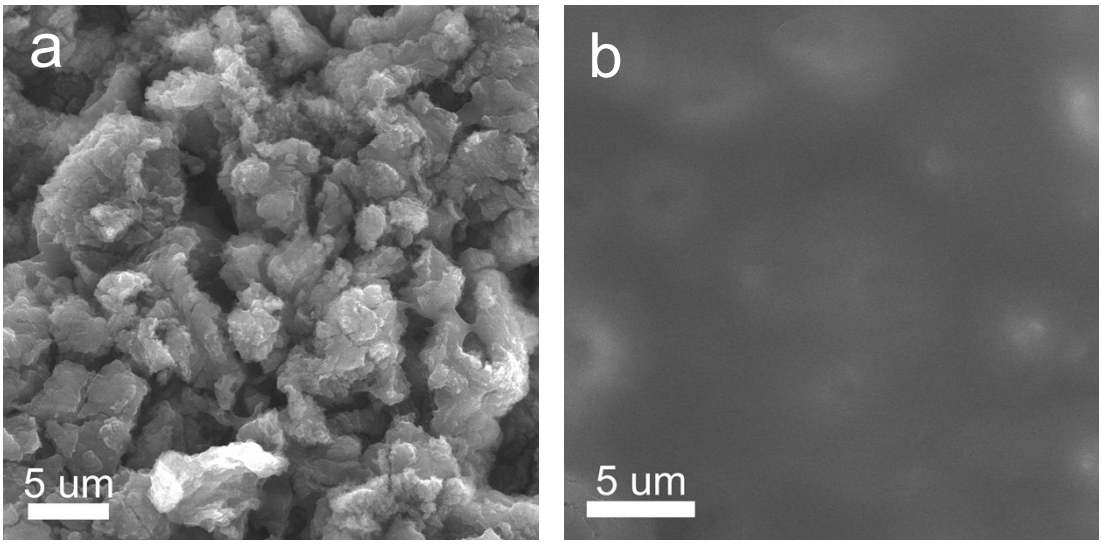

Figure S16 The SEM image of lithium metal with SPE (a) after 400 h and CPE-3%-BNNSs (b) after 1000 h at the current density of 0.1 mA cm-2 in symmetric cells

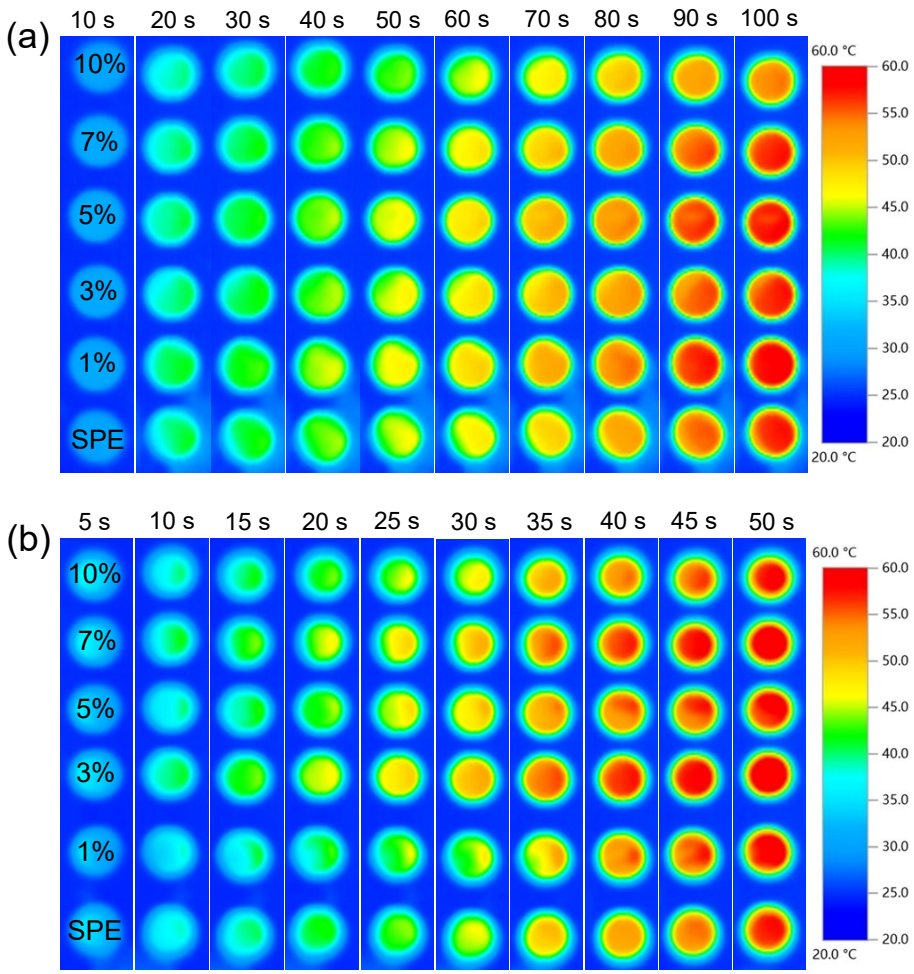

Figure S17 Infrared thermography images of CPE-*h*-BN (a) and CPE-BNNSs (b) with different addition of h-BN and BNNSs

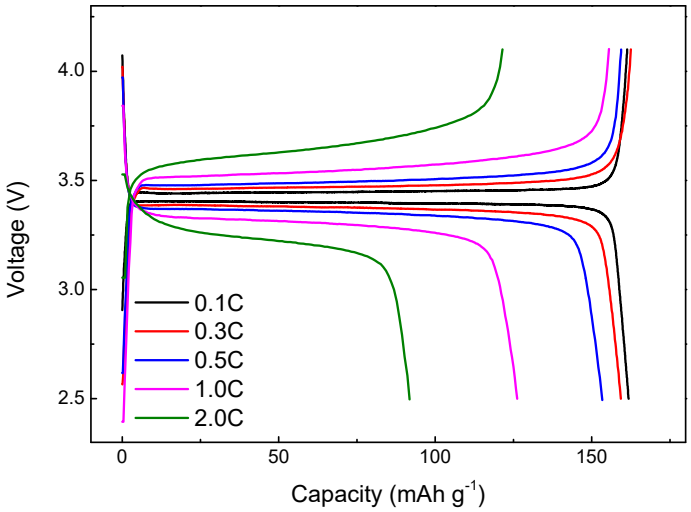

Figure S18 Charge and discharge curves at different rates: 0.1, 0.3, 0.5, 1.0 and 2.0 C with CPE-3%-BNNSs at 60 °C

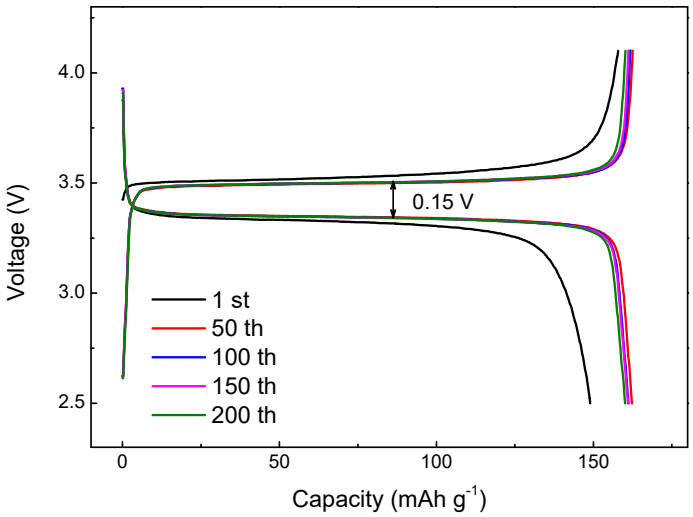

Figure S19 Charge/discharge voltage profiles of 1st, 50th, 100th, 150th and 200th cycle with CPE-3%-BNNSs at 0.5 C

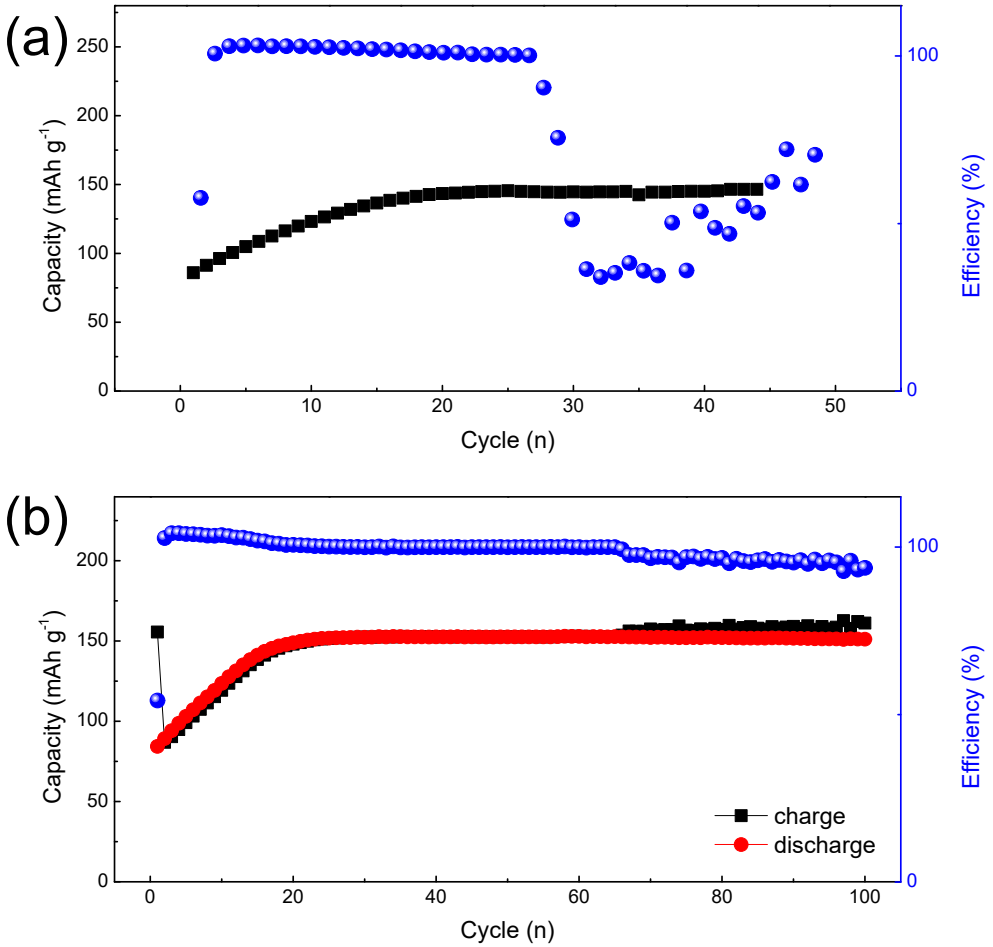

Figure S20 cycle performance of Li/LFP cells with SPE (a) and CPE-5%-*h*-BN at 0.5 C

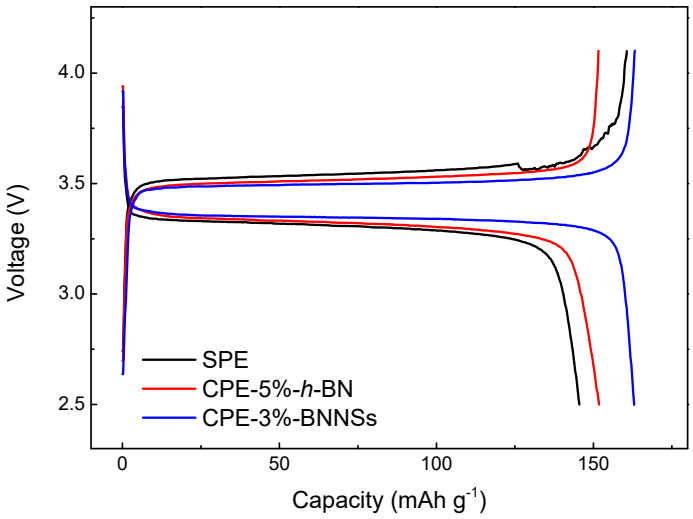

Figure S21 Charge/discharge voltage profiles of 25th cycle with SPE, CPE-5%-*h*-BN and CPE-3%-BNNSs at 0.5 C

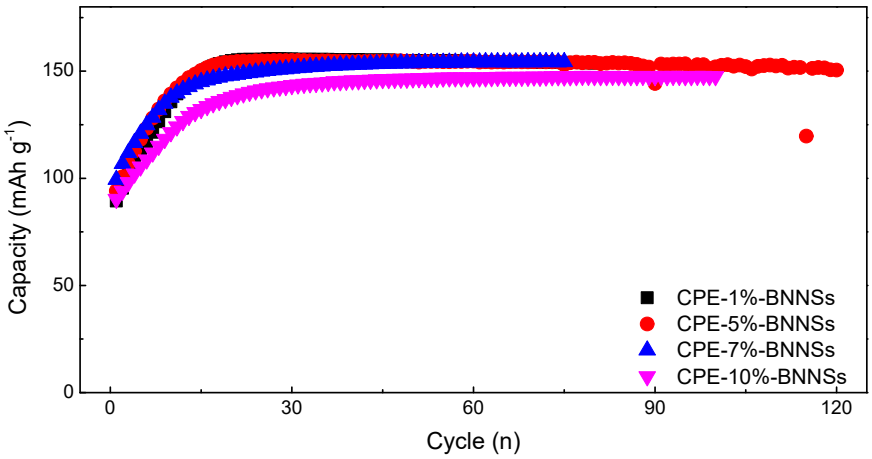

Figure S22 cycle performance of CPE-BNNSs with different BNNSs at 0.5 C

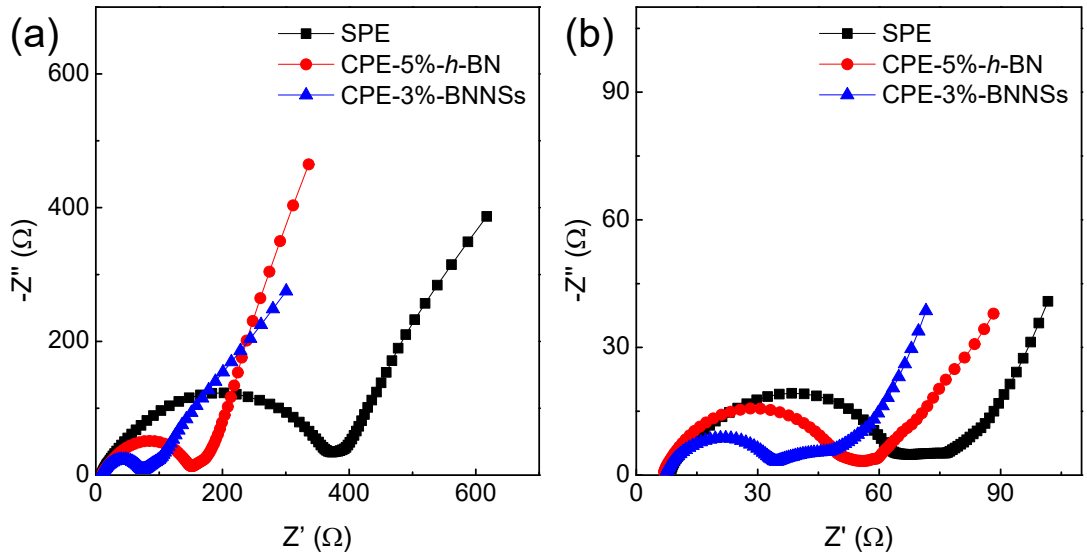

Figure S23 EIS spectra of Li/SPE/LFP, Li/CPE-5%-*h*-BN/LFP and Li/CPE-3%-BNNSs/LFP cell before (a) and after (b) 20 cycles at 0.5 C

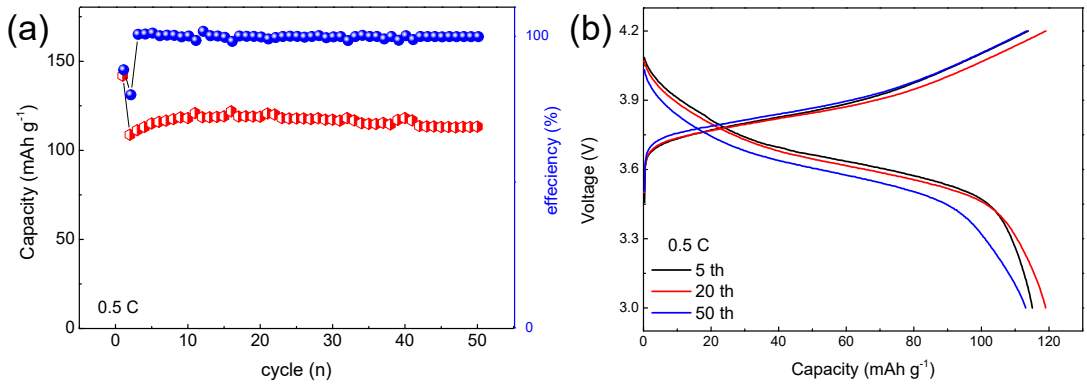

Figure S24 The cycle performance (a) and charge/discharge voltage profiles of 5 th, 25 th and 50 th cycle of Li|NCM622 based CPE-3%-BNNSs at 0.5C.

Table S1 The crystal face index (h k l), full width at half maxima (FWHM) and grain size (D) of h-BN and BNNSs

	hkl	FWHM	D/Å
h-BN	(0002)	0.186	520
BNNSs	(0002)	0.141	58

Table S2 Calculation of ion transfer numbers of SPE, CPE-h-BN and CPE-BNNSs electrolytes based on parameters obtained from EIS and DC polarization measurements

.

	I_0 / mA	I_{ss} / mA	R_0 / Ω	R_{ss} / Ω	t_{Li^+}
SPE	0.1341	0.0958	70.03	64.57	0.11
CPE-1%-*h*-BN	0.1048	0.06685	86.6	84	0.13
CPE-3%-*h*-BN	0.1852	0.08936	43.75	43.41	0.15
CPE-5%-*h*-BN	0.09499	0.06771	95.43	96.94	0.19
CPE-7%-*h*-BN	0.06364	0.05003	148.99	148.56	0.16
CPE-10%-*h*-BN	0.05359	0.03484	174.99	175.29	0.1
CPE-1%-BNNSs	0.0739	0.05709	124.05	120.37	0.21
CPE-3%-BNNSs	0.08264	0.06384	111.02	116.24	0.25
CPE-5%-BNNSs	0.07202	0.04745	122.38	127.83	0.2
CPE-7%-BNNSs	0.07789	0.0557	117.59	114.43	0.17
CPE-10%-BNNSs	0.05627	0.03753	162.86	161.96	0.14

Table S3 Impedance parameters of SPE, CPE-5%-h-BN and CPE-3%-BNNSs based Li/LFP batteries

	R_0 (Ω)	R_{ct} (Ω)
SPE	7.57	190.89
CPE-5%-*h*-BN	11.82	295.86
CPE-3%-BNNSs	7.72	40.34

Table S4. Rate performance of LFP/Li ASSBs with CPE-3%-BNNSs electrolyte in this work compared with previously reported in the literatures

electrolyte	Specific capacity retention ($mAh \cdot g^{-1}$) at different current density (C)			Ref.
CPE-3%-BNNSs	0.5	1.0	2.0	This work
	161.5	145.6	88.7	
PEO/LiTFSI/PI CSPE	0.3	0.5	1.0	[1]
	144.1	142.1	139.1	
SSPE-30	0.2	0.5	1.0	[2]
	85.4	59.3	44.7	
NCN-CPE	0.2	0.5	1.0	[3]
	163.4	152.2	124.4	
CSSE-1115	0.5	0.8	1.0	[4]
	136.5	122.7	113.2	
LLTO/PVDF-CPEs	0.5	1.0	2.0	[5]
	120	107	77	
PC-30	0.5	1.0	2.0	[6]
	121.6	92.5	65.4	
ANF-LATP-PEO-LiTFSI	0.3	0.5	1.0	[7]
	125	119	100	

Notes and Reference

[1] Y. Li, Z. Fu, S. L, X. Sun, X. Zhang, L. Weng, Polymer nanofibers framework composite solid electrolyte with lithium dendrite suppression for long life all-solid-state lithium metal battery, Chem. Eng. J., 2020 **440** 135816.

[2] C. Cao, Y. Li, S. Chen, C. Peng, Z. Li, L. Tang, Y. Feng, W. Feng, Electrolyte-solvent-modified alternating copolymer as a single-ion solid polymer electrolyte for high-performance lithium metal batteries, ACS Appl. Mater. Interfaces, 2019 **11** 35683-35692.

[3] R. Fan, W. Liao, S. Fan, D. Chen, J. Tang, Y, Yang, C. Liu, Regulating interfacial Li-ion transport via an integrated corrugated 3D skeleton in solid composite electrolyte for all-solid-state lithium metal batteries, Adv. Sci., 2022 **9** 2104506.

[4] H. Li, W. Liu, X. Yang, J. Xiao, Y. Li, L. Sun, X. Ren, P. Zhang, H. Mi, Fluoroethylene carbonate-Li-ion enabling composite solid-state electrolyte and lithium metal interface self-healing for dendrite-free lithium deposition, Chem. Eng. J., 2021 **408** 127254.

[5] B. Li, Q. Su, L. Yu, S. Dong, M. Zhang, S. Ding, G. Du, B. Xu, Ultrathin, flexible, and sandwiched structure composite polymer electrolyte membrane for solid-state lithium batteries, J. Membrane Sci., 2021 **618** 118734.

[6] T. Feng, Y. Hu, L. Xu, J. Huang, S. Hu, L. Zhang, L. Luo, Improving the cyclability of solid polymer electrolyte with porous V_2O_5 nanotube filler, Mater. Today Energy, 2022 **28** 101062.

[7] L. Liu, D. Zhang, T. Yang, W. Hu, X. Meng, J, Mo, W. Hou, Q. Fan, K. Liu, B. Jiang, L .Chu, M. Li, Flexible ion-conducting membranes with 3D continuous nanohybrid networks for high-performance solid-state metallic lithium batteries, J. Energy Chem., 2022 **75** 360-368.